Nat. Hazards Earth Syst. Sci., 15, 2425–2437, 2015
www.nat-hazards-earth-syst-sci.net/15/2425/2015/
doi:10.5194/nhess-15-2425-2015

Natural Hazards and Earth System Sciences Open Access EGU

Repeated glacial lake outburst flood threatening the oldest Buddhist monastery in north-western Nepal

J. Kropáček[1,2], N. Neckel[1,a], B. Tyrna[1,3], N. Holzer[2], A. Hovden[4], N. Gourmelen[5,6], C. Schneider[7], M. Buchroithner[2], and V. Hochschild[1]

[1]Department of Geography, University of Tübingen, Ruemelinstr. 19–23, 72070 Tübingen, Germany
[2]Institute for Cartography, Dresden University of Technology, Helmholtzstr. 10, 01069 Dresden, Germany
[3]Geomer GmbH, Im Breitspiel 11b, 69126 Heidelberg, Germany
[4]Department of Culture Studies and Oriental Languages, University of Oslo, Niels Henrik Abels vei 36, 0371 Oslo, Norway
[5]Institut de Physique du Globe de Strasbourg, Université de Strasbourg, 5 Rue René Descartes, 67084 Strasbourg CEDEX, France
[6]School of Geosciences, University of Edinburgh, Geography Building Drummond Street, Edinburgh, EH8 9XP, UK
[7]Department of Geography, RWTH Aachen University, Templergraben 55, 52056 Aachen, Germany
[a]now at: Alfred Wegener Institute, Helmholtz Centre for Polar and Marine Research, Bremerhaven, Germany

Correspondence to: J. Kropáček (jan.kropacek@uni-tuebingen.de)

Received: 15 October 2014 – Published in Nat. Hazards Earth Syst. Sci. Discuss.: 17 November 2014
Revised: 17 August 2015 – Accepted: 4 September 2015 – Published: 26 October 2015

Abstract. Since 2004, Halji village, home of the oldest Buddhist Monastery in north-western Nepal, has suffered from recurrent glacial lake outburst floods (GLOFs). A sudden englacial drainage of a supraglacial lake, located at a distance of 6.5 km from the village, was identified as the source of the flood. The topography of the lake basin was mapped by combining differential Global Positioning System (DGPS) measurements with a structure-from-motion (SFM) approach using terrestrial photographs. From this model the maximum filling capacity of the lake has been estimated as $1.06 \times 10^6\,m^3$ with a maximum discharge of $77.8\,m^3\,s^{-1}$, calculated using the empiric Clague–Mathews formula. A simulation of the flooded area employing a raster-based hydraulic model considering six scenarios of discharge volume and surface roughness did not result in a flooding of the village. However, both the village and the monastery are threatened by undercutting of the river bank formed by unconsolidated sediments, as it already happened in 2011. Further, the comparison of the GLOF occurrences with temperature and precipitation from the High Asia Reanalysis (HAR) data set for the period 2001–2011 suggests that the GLOF is climate-driven rather than generated by an extreme precipitation event. The calculation of geodetic mass balance and the analysis of satellite images showed a rapid thinning and retreat of Halji Glacier which will eventually lead to a decline of the lake basin. As the basin will persist for at least several years, effective mitigation measures should be considered. A further reinforcement of the gabion walls was suggested as an artificial lake drainage is not feasible given the difficult accessibility of the glacier.

1 Introduction

Glacier thinning and retreat in the Himalayas has resulted in the formation of a number of inherently unstable glacial lakes in the region (ICIMOD, 2011; Nie et al., 2013). The sudden catastrophic release of water from such lakes leads to extensive damage and often to casualties in the valley downstream (e.g. Haeberli, 1983; Björnsson, 1992; Huggel et al., 2002). The ice-dammed lakes are usually drained through a tunnel incised into the basal ice, by ice-marginal drainage or by mechanical failure of a part of the dam (Walder and Costa, 1996). Although it is known that glacial lake outburst floods (GLOFs) occur mainly after the onset of the snowmelt sea-

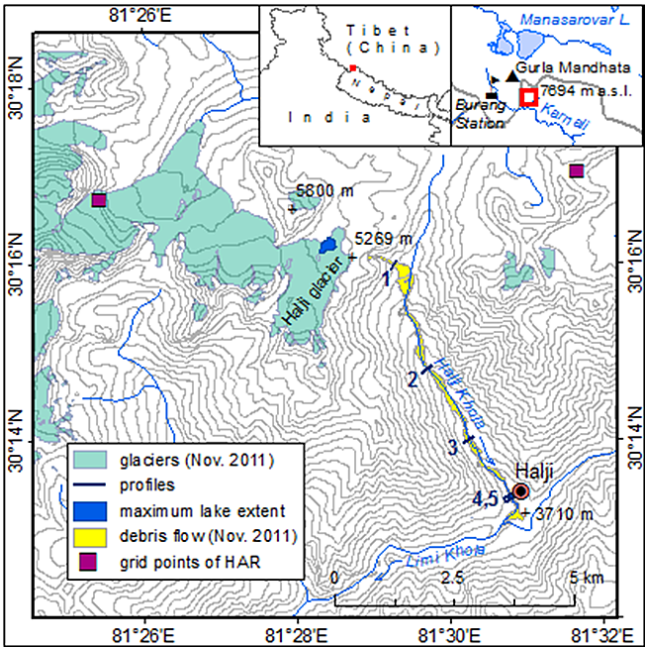

Figure 1. The study area in north-western Nepal. The extent of the debris flow was delineated from a high-resolution image from November 2011 available on Bing Maps.

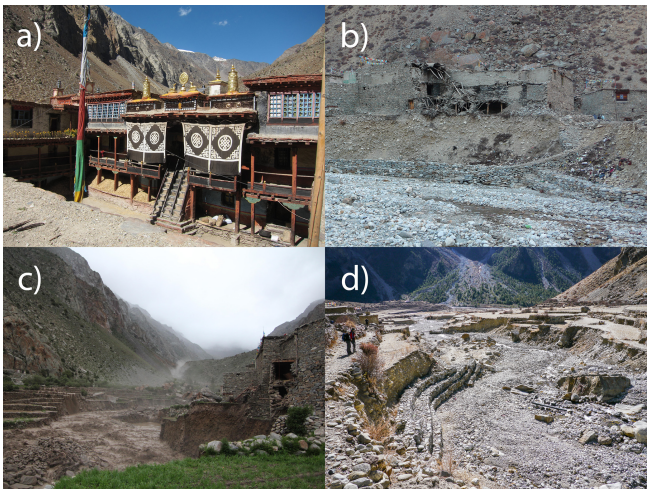

Figure 2. The Halji Glacier can be seen on the horizon above Rinchen Ling Monastery in **(a)**. Unconsolidated sediments of the alluvial fan which form the river bank in Halji and houses destroyed by the flood in 2011 can be seen in **(b)**. Swollen waters of Halji Khola during the flood on 30 June 2011 are captured in **(c)**. Eroded banks of Halji Khola at Halji village were reinforced by a gabion wall (photo taken in November 2013; **d**).

son (Haeberli, 1983), reliable prediction of the timing is difficult (Ng and Liu, 2009). Further, the mechanisms and circumstances of glacial flood release are still largely unknown (Fountain, 2011). For an estimation of the peak discharge of the tunnel-like drainage an empirical power-law relation was proposed by Clague and Mathews (1973), but its application to other types of floods can lead to significant underestimation (Walder and Costa, 1996). In some cases the total discharge volume can reach several km^3 (Walder and Costa, 1996). However, even discharges as small as $10\,m^3\,s^{-1}$ can be destructive, especially if they trigger a debris flow (Haeberli, 1983; Driedger and Fountain, 1989).

Since 2004, Halji village in north-western Nepal has been affected by periodic flooding occurring at the beginning of summer. The village is located in the Limi Valley at the southern slopes of the Gurla Mandhata Massif at an altitude of 3740 m above sea level (a.s.l.) (Fig. 1). So far the floods have washed away a large part of arable land and damaged several houses on the western margin of the settlement. Rinchen Ling Monastery, which is located only about 30 m from the damaged zone, plays a central role in the local community and has significant value as cultural heritage (Bidari, 2004; Hovden, 2013, Fig. 2a). Recent research shows that the monastery dates back to the beginning of the eleventh century (Hovden, 2013) and it is thus one of the oldest Tibetan Buddhist monasteries in Nepal. The whole village is built on a flat alluvial fan of the Halji River (Halji Khola) formed by unconsolidated alluvial sediments (Fig. 2b). Future flooding thus could represent a threat to both the village and the monastery.

Limi Valley is located at the southern margin of the Tibetan Plateau. The climate of the region, which can be classified as "Dwc" after Köppen (Peel et al., 2007), is characterized by cool summers and dry winters. Climate parameters measured at the closest meteorological station in Burang (3901 m a.s.l.) are shown in Fig. 3. A fast retreat of glaciers in the north-western part of Gurla Mandhata in the last decades was reported by Yao et al. (2007) and Holzer et al. (2015).

The objective of this study is to investigate the supraglacial lake basin as the source of the flooding and to determine its evolution and drainage mechanism (Sects. 4.1 and 4.2). To understand the timing and impact of GLOF events in Halji, the maximum discharge is estimated for various filling levels including the maximum level considering the present shape of the basin. Potentially flooded areas are delimited considering various scenarios in terms of maximum discharge and surface roughness (Sect. 4.3). As GLOF events are related to glacier dynamics, a further objective is to investigate the changes in glacier area and volume in the last decade. Further, we investigated modelled temperature and liquid precipitation during the period of lake filling to understand the driving factors of the flood occurrence (Sect. 4.4). Finally, with regard to possible GLOF events in the future, suitable mitigation measures are briefly discussed.

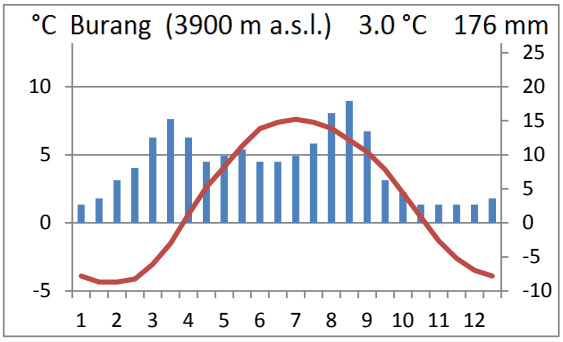

Figure 3. Climate diagram of Burang station located 30 km west from Halji Glacier after Miehe et al. (2001). Precipitation is indicated by the blue columns and temperature by the red curve.

2 History of the GLOFs in Halji

According to interviews with the local villagers, six GLOFs occurred between 2004 and 2014 (in 2004, 2006–2009 and 2011) (Diemberger et al., 2015). All GLOFs in Halji have taken place at the end of June or beginning of July. Whereas the exact dates of the early floods are not known, the timing of the most recent floods is very regular within a time span of approximately 1 week, as reported by the local people. The reports about the flood intensity in the particular years given by the local inhabitants are somewhat divergent, but the intensity of the floods seems to have increased over time. The flood on 30 June 2011, which was the largest so far, is well documented by photos and videos taken by one of the authors, who was an eyewitness of the event (e.g. Fig. 2c). The stream level in the village rose early in the afternoon and stayed high for several hours. The glacier flood evolved into a debris flow which covered the bottom of the valley with a layer of sediment, reaching several metres of thickness (Fig. 1).

Based on local observations by the authors, some technical measures were taken after the first floods in order to prevent future damage of the settlement. In 2010, a gabion wall was constructed along the east bank of the stream above and in the village. Its damaged parts were replaced after the flood in 2011 and further extensions of the wall were made in 2014.

After the flood in 2009, a team of local villagers attempted a climb of the glacier in order to search for the source of the flood. They reported that they discovered a small lake partly covered by ice (Diemberger et al., 2015). High-resolution satellite imagery acquired in November 2011 available through Bing Maps (http://www.bing.com/maps/), revealed a basin-like structure on the northern side of the glacier tongue. It seemed likely that this basin would be filled by meltwater forming a supraglacial lake with sufficient volume to cause the reported floods.

3 Materials and methods

3.1 Identification of the lake and mapping of the glacier extent from satellite data

In order to identify the source of the flooding we checked a number of satellite image archives for the period from April to September. The number of useful images for this period is limited due to persistent cloud cover related to the monsoon. Thus the lake could be detected only on three Landsat images.

To understand the circumstances of the GLOF events, changes in the extent of the Halji Glacier in the last decade were mapped using two cloud-free satellite images from Landsat-7 with a ground resolution of 30 m. The scenes were acquired by the Enhanced Thematic Mapper Plus (ETM+) sensor on 13 October 2001 and 26 November 2011. The glacier body was delimited using a band ratio of bands 3 and 5 (i.e. RED/SWIR) and a subsequent threshold application, which is an effective approach also in shadowed areas (Paul and Kääb, 2005). As the scene from 2011 shows some "SLC-off" artefacts (NASA, 2004) manual editing was needed to eliminate narrow data gaps crossing the glacier. The dates of the floods were provided by the leader of the local flood mitigation committee and through interviews with representatives from all 85 households in the village made by one of the authors during her 12 months' research stays between 2010 and 2012. Some of her findings are discussed in more detail in Diemberger et al. (2015). The dates were confirmed through further interviews conducted by three other authors during the field campaign in 2013.

3.2 Mapping of the lake basin topography

In order to get detailed information about the lake basin morphology, the empty lake was surveyed by means of 130 differential Global Positioning System (DGPS) measurements. The measurements were conducted in and around the basin in stop-and-go mode with a reference station on solid rock. Additionally, a dense point cloud was generated from a structure-from-motion (SFM) approach (Snavely et al., 2008; Westoby et al., 2012).

For this we employed the freely available VisualSFM software (e.g. Wu, 2011). As an input we used 161 images taken during the 2013 field campaign with an off-the-shelf Pentax K100D Super camera. The great advantage of the SFM technique compared to conventional photogrammetry is that scene geometry, camera positions and orientation are solved automatically by a redundant approach based on automatically detected features in the overlapping images (Snavely et al., 2008; Westoby et al., 2012). In a first processing step, VisualSFM creates a sparse point cloud and shows the approximated camera positions in a graphical interface (Fig. 4a). In a second processing step a dense point cloud is generated. As no ground control points (GCPs) were used

Table 1. Scenarios of the glacial lake outburst flood (GLOF) considering various discharge volumes at the glacier and surface roughness values.

Scenario	% of lake volume	total discharge volume (m^3)	Q_{max} ($m^3\,s^{-1}$)	Time to peak (h)	Roughness ($m^{1/3}\,s^{-1}$)
S1	125	1 320 000	90.0	8.3	20
S2	100	1 056 000	77.8	7.7	20
S3	75	792 000	64.2	7.0	20
S4	125	1 320 000	90.0	8.3	30
S5	100	1 056 000	77.8	7.7	30
S6	75	792 000	64.2	7.0	30

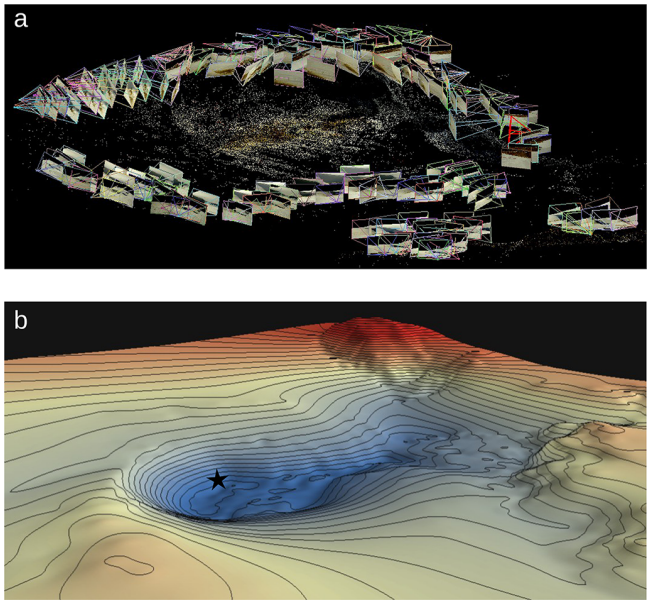

Figure 4. Terrain reconstruction of the lake basin based on a combination of structure-from-motion (SFM) approach using terrestrial photographs and differential Global Positioning System (DGPS) measurements. **(a)** Perspective view of the sparse point cloud and camera positions as seen from the North. **(b)** interpolated lake basin DEM (LB DEM) and contour lines as seen from the north-east. The contour interval is 2 m. Entrances to the englacial conduits are marked by a star.

so far, the dense point cloud is referenced to a relative coordinate system. In order to translate the dense point cloud to a metric coordinate system, we employed seven GCPs acquired by DGPS at the same time that the images were taken. Here we used the freely available SFM-georef Matlab package provided by James and Robson (2012). As the dense point cloud consists of millions of points we only used the mean value of points on a 1 m × 1 m grid for interpolating the lake basin DEM (LB DEM). Next to the SFM points we included 124 DGPS measurements in the final interpolation (Fig. 4b) leaving six DGPS measurements unemployed for an accuracy assessment of the final LB DEM. Compared to the well-distributed reference DGPS measurements, the LB DEM shows a mean and standard deviation of 0.22 ± 0.54 m.

The DEM of the lake basin allowed us to calculate the maximum filling capacity of the basin by summation of differences of the lake bottom elevations to the theoretical maximum lake elevation level and its multiplication by the pixel size of the LB DEM. The lowest point of the ice barrier was identified as maximum lake level elevation. To characterize the filling process, a hypsographic curve was generated. Peak discharge Q_{max} was calculated for various filling levels by applying the empirical power-law formula for tunnel-like discharge through an ice barrier proposed by Clague and Mathews (1973):

$$Q_{max} = 75 V_{max}^{0.67}, \quad (1)$$

where V_{max} is the discharge volume. The formula has a remarkably good fit for a large number of GLOFs to within an order of magnitude (Ng and Bjornsson, 2003). However, for a single lake, the exponent can differ significantly, as for instance in the case of Grímsvötn Lake in Iceland where it is equal to 1.83 (Björnsson, 1992).

3.3 Hydrodynamic modelling of GLOF scenarios

To study the dynamics of the outburst flood events and to assess the flood hazard for Halji village and the monastery, the two-dimensional raster-based hydrodynamic model FloodArea^{HPC} (Assmann et al., 2007; Geomer, 2012) was used to model different GLOF scenarios (Table 1). The scenarios are designed as combinations of one value of Q_{max} out of three values with one value of roughness out of two. These six scenarios allowed us to test the sensitivity of the results to the input parameters.

FloodArea^{HPC} was developed to model inundation areas for the Rhine atlas (ICPR, 2001) and has subsequently been used in modelling pluvial flooding, flash flooding and dam breaks. It is based on the Gauckler–Manning–Strickler formula and calculates flood depths in a cell by cell approach (Assmann et al., 2007), similar to the model developed by Bates and De Roo (2000). Flow velocity within a cell is calculated using the Gauckler–Manning–Strickler formula

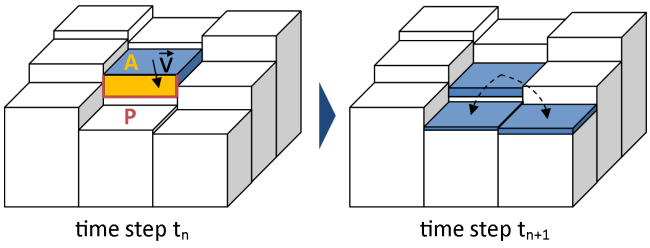

Figure 5. Schematic representation of the concept adopted in the FloodArea^{HPC} model. The block diagrams show the flow between raster cells in time steps t_n and t_{n+1}, indicating flow velocity vector $\boldsymbol{v}$, cross sectional area A and wetted perimeter P.

(Manning, 1891):

$$V = k_{St} \cdot R_h^{\frac{2}{3}} \cdot I^{\frac{1}{2}}, \quad (2)$$

where k_{St} is hydraulic roughness coefficient, R_h is hydraulic radius and I is inclination towards the lowest neighbouring cell. Hydraulic radius R_h is defined as the following ratio:

$$R_h = \frac{A}{P}, \quad (3)$$

where A is the cross-sectional area of flow and P the wetted perimeter (Fig. 5). In this model, water can flow from one raster cell to two neighbouring cells (Fig. 5) using the approach of Tarboton (1997) to determine flow directions. The duration of each calculation step and thus the duration of the simulation is determined by the exchange rate of water volume between cells in each iteration step. In this study, an exchange rate of 0.1 % was used.

In order to get reliable flood modelling results, topographical information should be as detailed as possible. For that reason a high-resolution Pléiades DEM with a spatial resolution of 1 m was obtained. Using the original DEM with a 1 m resolution as model input produced unrealistical slow water flow, which can be ascribed to artificial roughness from noise in the DEM, which is inherited to the stereo processing technique used in the generation of the DEM. To eliminate noise in the DEM, the raster was resampled to 2 m spatial resolution and a 3 × 3 low-pass filter was applied.

A crucial part of the model approach is the definition of an outflow hydrograph, which serves as input for the hydrodynamic model and should provide a realistic representation of lake outflow at the drainage tunnel outlet for a GLOF event. Due to the fact that nobody ever witnessed the drainage of the lake during a flood event, there are no data available to simulate a specific event, like the 2011 flood. Although numerical approaches can be used to model an outflow hydrograph for glacier dammed lakes (Vincent et al., 2010; Westoby et al., 2015), such models could not be applied here because most of the necessary parameters like drainage tunnel size, temperature or filling level of the lake are unknown. To approximate an outflow hydrograph for the scenarios, a log-normal

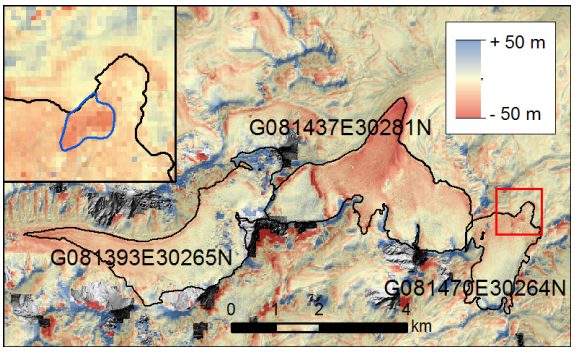

Figure 6. Image showing the difference between Pléiades DEM (2013) and SRTM DEM (2000) for mass balance calculation of glaciers G081470E30264N (Halji Glacier), G081437E30281N and G081393E30265N (glacier IDs are from Randolph Glacier Inventory). The detailed image for the northern part of Halji Glacier shows a deepening of the basin in the period between 2000 and 2013. The blue outline of the maximum lake extent is drawn as a reference.

distribution curve with a sigma value of 0.5 and a mean value of 0.0 was fitted to the outflow volumes and associated peak flows Q_{max}. This mathematical curve represents an approximation of the idealized curves described by Haeberli (1983) and Walder and Costa (1996). To check their plausibility, flood extents, flow depths and velocities were compared to the observations of the 2011 GLOF event. As there is no information available about the filling level of the lake before a GLOF event, different lake filling scenarios were defined (Table 1) to assess the potential flood hazard for Halji village by delineating potential inundation areas. To further investigate the model sensitivity, three different lake filling scenarios (75, 100 and 125 % of the maximum lake filling capacity) were calculated using two different Strickler roughness coefficients, resulting in six different simulations. The filling volume of 125 % represents a possible future extension of the basin.

3.4 Geodetic glacier mass balance from Pléiades satellite imagery

Geodetic glacier mass balance (Fig. 6) was determined for the period 2000–2013 by subtracting Shuttle Radar Topography Mission (SRTM) version 4.1 elevations from a more recent DEM derived from Pléiades tri-stereo imagery. Pléiades is a French high-resolution earth observation system composed of two satellites launched in 2011 and 2012. It offers in-track tri-stereoscopic image acquisition with a spatial resolution of 0.5 m (panchromatic) and a pixel depth of 12-bit (Astrium, 2012). Imagery of the study site was acquired on 26 October 2013.

We extracted a DEM at 1 m spatial resolution using the PCI 2013 Geomatica OrthoEngine software package and its rational functions model. DEM extraction is based on

Figure 7. View of the empty lake basin from the north **(a)**. The entrances to the en-glacial conduits draining the lake located at the lower edge of the toe of the ice barrier are marked by A. The supraglacial streams which lead meltwater to the basin are marked by B. The distance between A and B is approximately 170 m. A detailed view of the entrances to the en-glacial conduits is shown in **(b)**. A layer of the lacustrine sediment is visible in the lower right corner. Debris deposited by the floods in the middle part of the valley is presented in **(c)**.

ephemeris information and GCPs. A resampled version of this DEM was used for the hydrodynamic modelling. For the geodetic mass balance calculation, both DEMs were resampled to a resolution of 30 m before the subtraction. Elevation pixels with insufficient correlation coefficients (< 0.3) were ignored. This threshold proved to be most adapted to keep elevation pixels of fair quality in areas of high saturation. DEM co-registration to the SRTM reference is based on an analytical approach following Nuth and Kääb (2011) with remaining inaccuracies of 1.24 m in X and 1.50 m in Y. We observed a spatially varying elevation bias in form of a slight tilt with respect to SRTM. This was corrected by a two-dimensional linear trend surface to reduce the mean height offset on stable terrain to zero (Holzer et al., 2015).

Outlier detection and gap filling in the difference image to SRTM was employed independently for each glacier accumulation zone and each 25 m elevation band in the ablation zone following Holzer et al. (2015). The accumulation area is separated by the equilibrium line altitude (ELA) which was estimated as 5660 m a.s.l. for a nearby glacier (G081393E30265N, Randolph Glacier Inventory (RGI) ID, Pfeffer et al., 2014) by Shi (2008). Each pixel value determined to be an outlier using the 5 and 95 % quantiles was replaced by the mean of the values of all adjacent non-outlier pixels. Penetration of the SRTM C-band beam into glacier ice was corrected by a depth of 2.3 m for firn and snow (accumulation area) as well as 1.7 m for clean ice (ablation area) with an uncertainty of ± 0.6 m (Kääb et al., 2012). Glacier thinning and mass balance at a presumed ice density of $850 \pm 60\,\mathrm{kg\,m^{-3}}$ (Huss, 2013) was determined for Halji Glacier as well as its two neighbouring glaciers located further to the west. The precision of the DEM was estimated at 4.83 m from the normalized median absolute deviation (NMAD) (Höhle and and Höhle, 2009). The total error of glacier mass balance uncertainties was calculated as the root of the sum of each squared error term.

3.5 Correlation of GLOF occurrence with climate data

Hourly precipitation and temperature 2 m above the surface were derived from the High Asia Reanalysis (HAR) data set. The data correspond to a model cell representing the elevation of 5273 m a.s.l., located 4 km from the glacier to the west (Fig. 1). The model contains gridded fields of atmospheric variables with a resolution of 10 km for the Tibetan Plateau and surroundings (Maussion et al., 2014). Following the idea of a degree day model (Braithwaite, 1984) the hourly above-zero temperatures of the cell were cumulated for the period from January to June for each year between 2001 and 2011. The end of June corresponds to the outburst of the lake. The cumulative temperature thus represents a proxy for the volume of meltwater amount discharging from the glacier to the lake. Similarly, hourly precipitation from January to June (P_{cum}) was cumulated for temperatures above 0 °C representing liquid precipitation that contributes to the filling of the lake. The two variables T_{cum} and P_{cum} were compared with the flood occurrences. Further, single liquid precipitation totals were calculated from the hourly precipitation data to see what the discharge of an extreme precipitation into the lake is.

4 Results

4.1 Field campaign in November 2013

During the field campaign in November 2013 the existence of the temporary supra-glacial lake indicated by the satellite imagery was proved. A large empty basin was found at the northern side of the glacier tongue close to the terminus. Its bottom was covered by a thin layer of lacustrine sediments (Fig. 7b). Moreover, several entrances to en-glacial conduits were discovered along the south-eastern bottom edge of the basin at an altitude of 5292 m a.s.l. The entrances were partially covered by snow and sediments and their total cross section was estimated to be 5–15 $\mathrm{m^2}$. Close to the entrance,

Table 2. Dates of glacier lake presence detected on Landsat images and occurrence of glacial lake outburst floods (GLOF) in respective years.

	GLOF	Lake before 1 Jul	No lake	Images checked
2004	yes	–	–	1
2005	–	–	6 Sep	2
2006	yes	–	9 Sep	1
2007	yes	8 Jun	12 Sep	2
2008	yes	–	–	0
2009	23 Jun	5, 21 Jun	17 Sep	6
2010	–	–	28 Sep	3
2011	30 Jun	–	–	7
2012	–	–	–	3
2013	–	–	23 May	10
2014	–	–	3 Jun	14

the channels were filled with ice, forming a horizontal level showing that the channels were blocked and filled with water before the freeze-up. These conduits drain the lake towards an outflow on the south-eastern edge of the glacier, covering a distance of 500 m. The entrances clearly follow a shear crack predisposed probably by a discontinuity between ice layers. This is in agreement with findings of Fountain et al. (2005) and Gulley (2009) who showed that en-glacial conduits in temperate glaciers follow glacio-structural features such as ice fractures rather than developing a passage through the ice mass of a higher conductivity as presumed in the past (Shreve, 1972).

4.2 Glacier changes and evolution of the lake basin

The first evidence of an ice-dammed basin on the Halji Glacier was found on aerial images from the archive of the Survey Department in Kathmandu acquired in 1996. However, the structure was covered by snow and it is not possible to say whether it contained a lake or not. The lake could be detected only on Landsat images from 8 June 2007 acquired by Thematic Mapper (TM), and from 5 and 21 June 2009 acquired by the Enhanced Thematic Mapper (ETM+) sensor (Fig. 8, Table 2). For seven Landsat scenes acquired mainly in September, it could be stated that the lake was not present. The rest of the Landsat images as well as other available high-resolution images were either cloud-covered or showed snow-covered surfaces where the lake basin is located.

The change in extent of the Halji Glacier in the period 2001–2011 is shown in Fig. 12. The glacier front retreated for up to about 80 m in the vicinity of the lake and for about 50 m at the subglacial channel outlet. The changes in glacier thickness for the period 2000–2013 are shown in Fig. 6. Table 4 presents changes in glacier mean elevation and in total ice volume as well as the mean annual mass balance for the Halji Glacier and two other glaciers located further to the

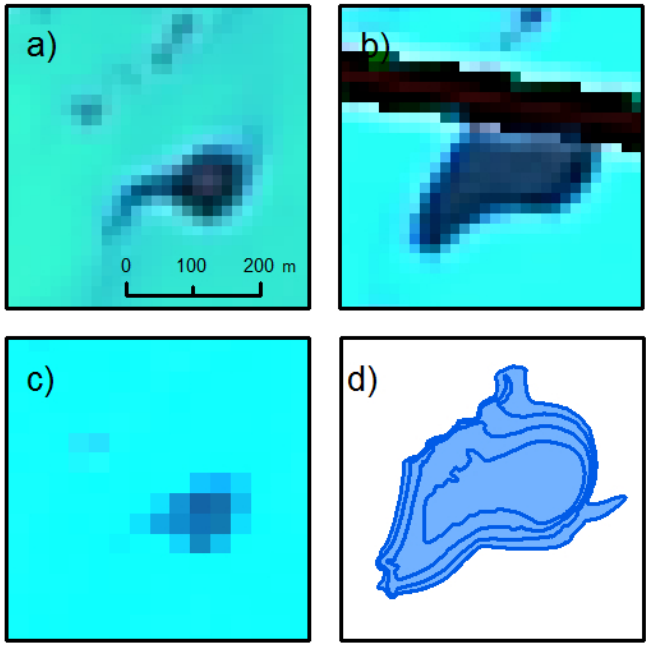

Figure 8. The supraglacial lake on Landsat images (RGB combination of bands 5, 4 and 3) acquired on 8 June 2007 **(a)**, 24 June 2007 **(b)** and 5 June 2009 **(c)**. The image from 24 June 2007 is affected by a data gap due to SLC-off artefacts. Lake extents for 25, 50, 75 and 100 % of the maximum filling capacity corresponding to 14.4, 18.8, 21.8 and 24.1 m of lake depth, respectively, are shown in **(d)**.

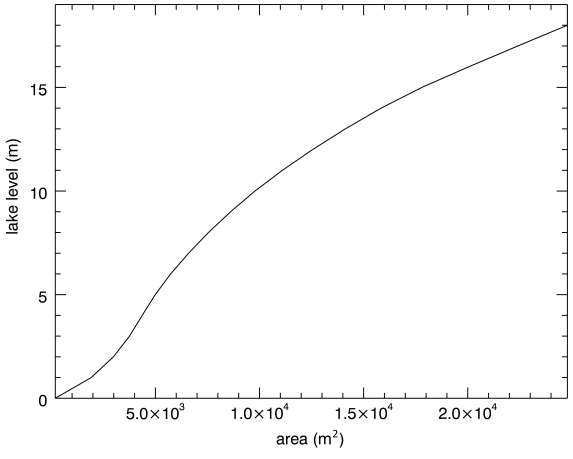

Figure 9. Hypsographic curve of the lake basin derived from the detailed DEM (LB DEM) showing the relation of the lake depth and the lake area.

west. The detailed image of glacier thinning for the surroundings of the lake basin (Fig. 6) shows a distinct area of a high mass loss in the area of the basin reaching up to around 30 m. This means that the basin developed mainly between 2000 and 2013. The morphology of the lake basin as reconstructed by DGPS and SFM is shown in Fig. 4. It appears that the

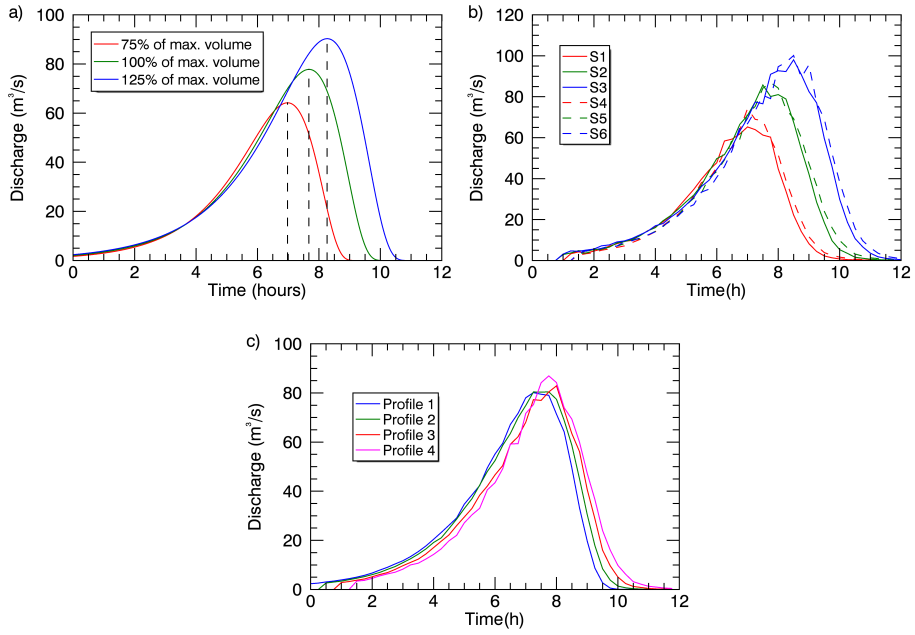

Figure 10. (a) Lake outflow hydrographs for three different filling levels (100, 75 and 50 % of lake volume) which were used as input for the hydrodynamic modelling. **(b)** Modelled discharge curves for profile 4 next to the village for different lake volumes and different roughness parameters according to Table 1 (for the location of profile 4 see Fig. 1 and 11); **(c)** modelled discharge curves of S2 scenario for profiles 1–4 show the downstream propagation of the flood wave.

glacier ice barrier that blocks the basin is 24 m high at its lowest point. To understand the relation between the lake depth and its volume, a hypsometric curve was derived for the basin (Fig. 9). The maximum volume of the basin before the overtopping of the barrier in the south-east is 1.06×10^6 m^3.

4.3 Flow discharge and flood extent

The lake area, volume and peak discharge calculated after Clague and Mathews (1973) is given in Table 3. The area of the glacier that drains to the lake basin is 1.12 km^2 and the whole basin including the off-glacier area is 1.46 km^2.

The results of the hydrodynamic modelling of the six defined scenarios are illustrated in Figs. 10b, c (discharge curves) and 11 (flood extents). The discharge curves generated by the model FloodArea^{HPC} (Fig. 10b) show for all scenarios a slowly rising limb and a steep falling limb, just as the lake outflow hydrographs (Fig. 10a) that were used as model input. Peak discharge at the village is slightly higher than the input peak discharge at the outflow of the lake. In the following, the influence of input parameters (discharge volume/peak discharge and roughness coefficients) on the model results is described.

As expected, the choice of the roughness parameter has an influence on flow velocity, which is observable in the delayed arrival of the flood for the high roughness ($k_{st} = 20\,\mathrm{m}^{1/3}\,\mathrm{s}^{-1}$) scenarios as compared to the low roughness ($k_{st} = 30\,\mathrm{m}^{1/3}\,\mathrm{s}^{-1}$) scenarios (Fig. 10b). In the high roughness scenarios, the recession of the hydrograph begins about 10 min later than in the low roughness scenarios. Figure 10c shows that the travel time of the flood wave peak from profile 1 to profile 4 takes 30 min in the S2 scenario (100 % lake volume, $k_{st} = 20$). Given a flow distance of 5700 m between profile 1 and 4, mean flow velocity is 3.2 m s^{-1}. For the S4 scenario, travel time is about 15 min and mean flow velocity is 6.4 m s^{-1}. The value range of 3.2–6.4 m s^{-1} seems reasonable and corresponds to the value range of 3–6 m s^{-1} by O'Connor et al. (2001) for lake outbursts which induce debris flows.

There is also an effect of roughness values on discharge and flood depths. Due to the fact that mean flow velocities are higher with lower roughness ($30\,\mathrm{m}^{1/3}\,\mathrm{s}^{-1}$), flow discharge is also slightly higher (Fig. 10b). Accordingly, in the low roughness coefficient scenarios (S4–6) the maximum flow depths at the village are 0.3 m lower than in the higher rough-

Table 3. Area, volume and peak discharge for different water levels in the basin, calculated using the lake basin DEM (LB DEM).

Elevation (m a.s.l.)	Level (m)	Area (m^2)	Volume (10^6 m^3)	Q_{max} (m^3 s^{-1})
5297	5	6368	0.03	6.33
5302	10	12552	0.12	17.70
5307	15	24280	0.29	32.97
5312	20	43684	0.63	55.22
5316	24	64328	1.06	77.81

Table 4. Glacier mean elevation, total ice volume change and annual glacier mass balance measured from DEM difference between SRTM-3 (2000) and Pléiades (2013). For details on the uncertainty intervals, see Sect. 3.4.

Glacier/GLIMS ID	Mean elevation change (m)	Volume change (Gt $\times 10^{-3}$)	Annual mass balance (m w.e.a^{-1})
Halji Glacier	-6.6 ± 4.9	-15.8 ± 11.6	-0.40 ± 0.30
G081437E30281N	-13.9 ± 4.9	-92.0 ± 32.9	-0.84 ± 0.30
G081393E30265N	-3.2 ± 4.9	-18.8 ± 28.7	-0.19 ± 0.30

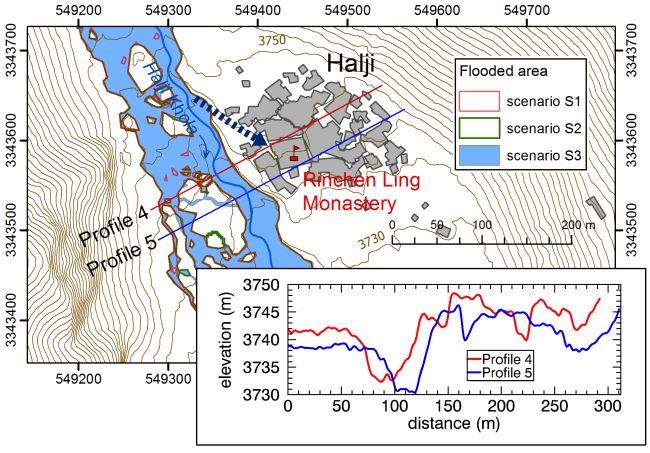

Figure 11. The simulated flooded area in the vicinity of Halji village assuming three different peak discharge values and a roughness value of 20. The passage between houses leading to the monastery is shown as a dashed blue arrow. Coordinate system: UTM, zone 44° N; datum: WGS 84.

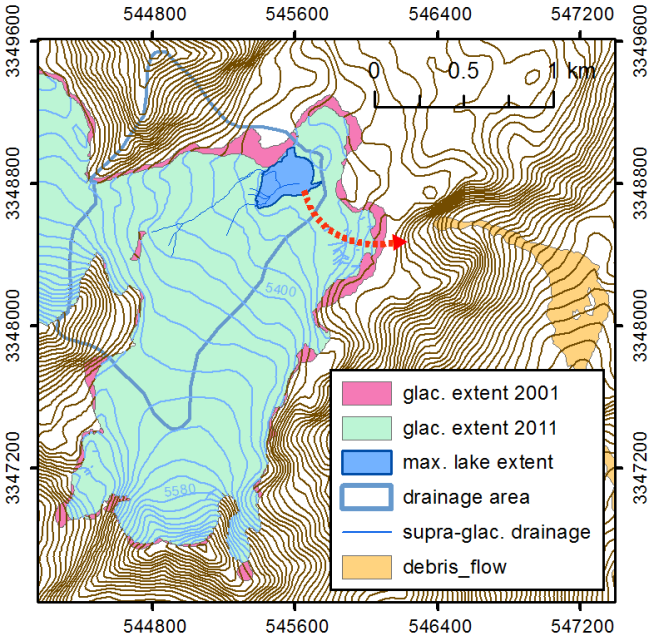

Figure 12. Changes in the extent of the Halji Glacier in the period from 2001 to 2011 as detected from Landsat images. Drainage of the supraglacial lake during the GLOF event is shown as a dashed red arrow. Coordinate system: UTM, zone 44° N; datum: WGS 84.

ness scenarios (S1–3). This is mainly because with higher roughness, more water accumulates, whereas with a lower roughness value, discharge is faster and there is less flow accumulation. Although the choice of roughness values has an effect on flow velocities, flood depths and discharge, there is no noticeable effect of roughness values on flood extents.

Considering the different lake filling scenarios (75, 100 and 125 % of the lake filling capacity), there are slight differences in flood extents, but the effect is not very strong (Fig. 11). At the eastern river bank facing the village, flood extents are almost identical because the embankment is steep and the flood stays within the channel (for details of the terrain see profiles in Fig. 11).

As the flood in 2011 came unexpectedly after no flood occurred in 2010, there were no measurements possible in the field. Anyhow, we could assess the modelled flow velocities, travel time and discharge using the available field data. Several photographs were taken during the flood. This allowed us to validate our results assuming that the modelled scenario with 100 % of the lake volume approximates the 2011 flood.

Regarding flood depths, it can be stated that the calculated maximum flow depth of 2.5 m for profile 4 in the village corresponds to the photos taken during the flood, albeit actual flow depths might have been slightly higher than modelled flow depths. The same applies for the simulated flood extent which corresponds to the photographs of the 2011 flood. According to the model results under all six scenarios, as well as during the 2011 flood, the water stayed in the channel in the vicinity of the village.

Modelled flow velocities of up to 9 m s^{-1} at the narrow sections of the channel for the S2 scenario seem plausible. According to the empirical Hjulström–Sundborg diagram (Sundborg, 1956), which represents the relationship between flow velocity and sediment particle size, this flow velocity would be high enough to erode blocks of up to 100 cm diameter. Transported and deposited blocks up to that size could be found downstream these narrow sections.

Table 5. Volume of liquid precipitation received in the area draining to the supraglacial lake each year until the end of June which was calculated using hourly precipitation and temperature data from the High Asia Reanalysis (HAR) data set. For comparison, the maximum filling capacity of the lake basin in 2013 was 1.06×10^6 m^3.

Year	V (10^6 m^3)
2001	0.51
2002	0.93
2003	0.71
2004	0.67
2005	0.90
2006	0.70
2007	0.60
2008	0.84
2009	0.46
2010	0.39
2011	0.94

4.4 Correlation of GLOF events with climate data

The comparison of the occurrence of the GLOF with the hourly cumulative above-zero temperature (Fig. 13a) shows a good match. Starting in 2003, the years with no flood appear to have a low T_{cum}. A similar pattern is present in the case of P_{cum}, although the dependency seems to be weaker. The high value of P_{cum} for the year 2011 corresponds to the strongest flood recorded so far.

The cumulated liquid precipitation gives us an idea if the supraglacial lake can be filled by mere precipitation amount received in the drainage basin of the lake. The theoretical run-off from liquid precipitation into the lake basin during the period in the respective summer season prior the GLOFs ranges from 0.50×10^6 to 0.93×10^6 m^3 (Table 5). This is a maximum value since it disregards any re-freezing in the glacier. The upper value corresponds to 88 % of the maximum filling volume of the lake. The maximum liquid precipitation event in the period 2001–2011 occurred on 19 September 2010 and it amounts to 60.2 mm. Disregarding refreezing, evaporation etc., this precipitation event could generate a run-off corresponding to 8.3 % of the lake basin volume.

5 Discussion

5.1 Lake basin evolution and its drainage

The appearance of the supraglacial lake on the Halji Glacier can be linked to the overall glacier retreat in the Himalayas in the last decades (Kääb et al., 2012, 2015; Bolch et al., 2012; Gardelle et al., 2013; Neckel et al., 2014). The evolution of the lake was likely induced by an undulation of the glacier surface that reflects an over-deepening of the glacier bed. The presence of the basin before the first GLOF event is not well documented due to an absence of useful satellite data. However, from the DEM difference, it is evident that the deepening of the basin must have occurred mainly between 2000 and 2013. The long life of the supraglacial basin is probably a result of a balance between glacier movement, glacier thinning and enlargement of the basin by thermal erosion of the lake water which absorbs more radiation than the surrounding ice due to its higher albedo.

The lake basin can fill up relatively quickly during June as documented by two Landsat images for the year 2007. The flood occurred each time within a range of a few days at the end of June/beginning of July. This suggests that the floods are rather climate-driven than triggered by extreme precipitation events. This is further supported by the coincidence of the GLOF events with high values of cumulative above-zero temperatures calculated from the HAR data set. It was shown that the lake basin can almost fill up merely with liquid precipitation accumulated until the end of June. Snow and glacier melting during June also depend on temperature. This means that in each year with a relatively warm June, a GLOF event may occur. The satellite images from May 2013 and June 2014 suggest that during the years without GLOF no lake develops in the basin. In these years water from the drainage area above the basin probably drains sub-glacially.

The entrances to the conduits found in the lake basin suggest that the lake discharge flows first en-glacially and further probably sub-glacially. This mechanism can be classified as a tunnel-like discharge that could be described for different filling levels by an empirical equation. However the maximum discharges computed can be largely exceeded if the conduits get blocked and then suddenly released as described by Ballantyne and McCann (1980) and Haeberli (1983). This means that larger floods than the maximum calculated flood cannot be ruled out. It should be noted that the maximum discharge of a single event can largely differ from the calculated value as the Clague–Mathews relation is statistically valid for a number of lake outbursts.

5.2 Flood hazard

The simulation of the flooded area assuming three values of maximum discharge from the lake did not result in flooding of the village. However, we observed during the field trip that houses in Halji are built on loose sediments of an alluvial fan. As such they are threatened by undercutting of the river bank by the flood. This mechanism led to a collapse of two of the houses next to the river during the flood in 2011. The monastery can be affected either by undercutting or if the stream loaded by sediment spills over the gabion wall and enters the alleys of the settlement. In this respect, one of the alleys is especially dangerous as it is inclined towards the village centre and leads from the river bank directly to the monastery (Fig. 11).

It has to be noted, that the applied model does not take into account processes such as erosion, sediment transport and deposition which also have an effect on flow veloci-

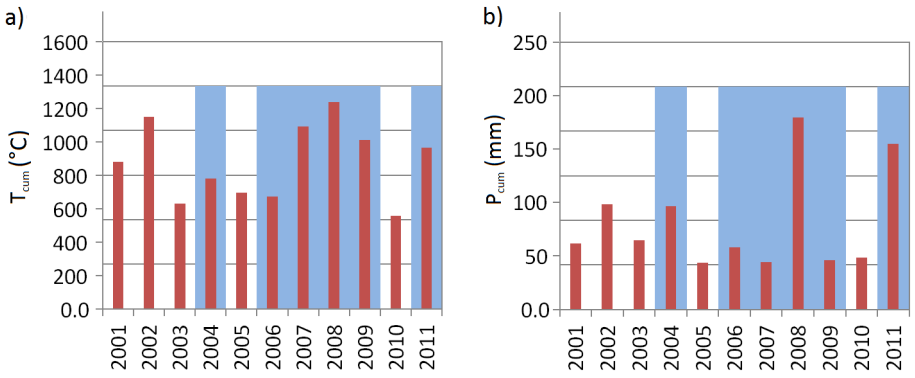

Figure 13. The **(a)** annual cumulative above-zero temperature T_{cum} and **(b)** annual cumulative precipitation P_{cum}, calculated for the period January to June, are given for hourly High Asia Reanalysis data (HAR) over the period 2001–2012. The precipitation was cumulated only for above-zero temperatures, thus it represents the liquid part of precipitation. The years with a GLOF event are marked by a blue column in the background.

ties. The application of a model that also includes the debris flow, induced obviously by the floods in Halji, would require many more comprehensive field data than were available in this study. Necessary data would include measurements of stream flow, pre- and post-flow topography, sediment load, grain size, etc. Breien et al. (2008) note that a main challenge in modelling debris flow induced by GLOFs is the change of flow characteristics due to the temporal and spatial variability of viscosity, cohesion, friction and collision rate.

5.3 Future perspective of the basin

Assuming a continuation of the glacier retreat detected from Landsat data and the negative mass balance, in the future the lake basin will eventually disappear due to the downwasting of the glacier leading to the elimination of the GLOF hazard for Halji village. Assuming the present climate conditions and the same retreat rate of the glacier margin as in the period from 2001 to 2011, the decline of the ice barrier could be roughly estimated to be 30 years. However it is possible that the size of the lake basin and the associated discharge volume still increase due to thermal erosion of water before the predicted decline of the basin.

5.4 Consideration of mitigation measures

This implies that in the near future, a similar or even larger GLOF event can occur. Suitable mitigation measures should be therefore considered, such as an artificial drainage of the lake. An adequate measure would be a construction of a drainage tunnel through the bedrock (e.g. Reynolds et al., 1998). This solution is clearly unfeasible, taking into account the remoteness of the place, lack of resources and the absence of access for the heavy machinery. A further obstacle is the ice bottom of the lake which would complicate the construction of the tunnel entrance. An installation of a siphon made of plastic tubes would be more feasible (e.g. Vincent et al., 2010); however, due to the low gradient of the eastern slope of the glacier barrier, such a pipe would have to be longer than 400 m. It seems more realistic to protect the village by measures along the downstream part of Halji Khola. The existing gabion walls protecting the riverbank in the village and upstream should be further reinforced. The common gabions used so far seem to be weak, as evident during the 2011 event. Larger gabions made of a thicker wire would have a better chance of resisting a large flood. Connection of the gabions and their anchoring would further improve the situation. A simple measure to preview the flood would be an ascent to the lake basin around mid-June to check visually whether the lake develops. This would provide valuable information about a possible burst. Further, an early warning system for Halji village should be considered.

6 Conclusions

The presented study shows how a combination of field measurements and satellite data analysis can help to assess hazards connected to the evolution of a glacial lake. The lake that seasonally develops on the Halji Glacier is relatively small compared to the large moraine dammed lakes in Nepal. Nevertheless, its discharge which leads to a debris flow presents a serious threat to both Halji village and the ancient Rinchen Ling Monastery.

It appears that even under present climate conditions, the glacier will retreat further, a development which will eventually lead to the decline of the lake basin. Nevertheless, it seems likely that the basin will persist for at least several more years. Therefore suitable mitigation measures should be considered to improve the flood resilience of Halji village.

Acknowledgements. This work was supported by the German Research Foundation (DFG) Priority Programme 1372, "Tibetan Plateau: Formation-Climate-Ecosystems" within the DynRG-TiP ("Dynamic Response of Glaciers on the Tibetan Plateau to Climate Change") project under the code BU 949/20-3 and SCHN 680/3-3, and by the German Federal Ministry of Education and Research (BMBF) Program "Central Asia – Monsoon Dynamics and Geo-ecosystems" (CAME) within the WET project ("Variability and Trends in Water Balance Components of Benchmark Drainage Basins on the Tibetan Plateau") under the codes 03G0804D, 03G0804E and 03G0804F. Pléiades imagery was received by the Institut de Physique du Globe and the ICube Laboratory (UMR 7357 CNRS) of the University of Strasbourg as part of the second run of the program RTU (Recette Thématique Utilisateurs) within the satellite program ORFEO (Optical and Radar Federation for Earth Observation) of the French Space Agency CNES and processed by the Institute of Cartography of the Dresden University of Technology, Germany (https://rtu-pleiades.kalimsat.eu).

The Landsat scenes were provided by the USGS and the SRTM-3 C-band DEM version 4.1 by the Consultative Group for International Agricultural Research (CGIAR). We thank the community of Halji and Benjamin Schröter from TU Dresden for their support during the field trip. Thanks to Gebhard Warth for his support with Landsat data processing. We acknowledge support by the Open-Access Publishing Fund of the University of Tübingen.

Edited by: B. D. Malamud
Reviewed by: A. Emmer and three anonymous referees

References

Assmann, A., Schroeder, M., and Hristov, M.: High Performance Computing for raster based modelling, Angewandte Geoinformatik 2007, Beiträge zum 19. AGIT-Symposium, Salzburg, Austria, 19–24, 2007.

Astrium: Pléiades Imagery – User Guide V2.0, Astrium GEO-Information Services, France, 5, rue des Satellites, BP 14359, 31030 Toulouse Cedex 4, France, 2012.

Ballantyne, C. and McCann, S.: Short-lived damming of a high-Arctic ice-marginal stream, Ellesmere Island, N. W. T., Canada, J. Glaciol., 25, 487–491, 1980.

Bates, P. and De Roo, A.: A simple raster-based model for flood inundation simulation, J. Hydrology, 236, 54–77, 2000.

Bidari, K.: Halji Monastery – a hidden heritage in North-West Nepal, Ancient Nepal, 155, 1–5, 2004.

Björnsson, H.: Jökulhaups in Iceland: prediction, characteristics and simulation, Ann. Glaciol., 16, 95–106, 1992.

Bolch, T., Kulkarni, A., Kääb, A., Huggel, C., Paul, F., Cogley, J. G., Frey, H., Kargel, J. S., Fujita, K., Scheel, M., Bajracharya, S., and Stoffel, M.: The State and Fate of Himalayan Glaciers, Science, 336, 310–314, doi:10.1126/science.1215828, 2012.

Braithwaite, R. J.: Calculation of degree-days for glacier-climate research, Zeitschrift fur Gletscherkunde und Glazialgeologie, 20, 1–8, 1984.

Breien, H., De Blasio, F., Elverhoi, A., and Hoeg, K.: Erosion and morphology of a debris flow caused by a glacial lake outburst flood, Western Norway, 5, 271–280, doi:10.1007/s10346-008-0118-3, 2008.

Clague, J. J. and Mathews, W. H.: The magnitude of jökulhaups, J. Glaciology, 12, 501–504, 1973.

Diemberger, H., Hovden, A., and Yeh, E.: The honour of the mountains is the snow: Tibetan livelihoods in a changing climate (forthcoming), in: The High-Mountain Cryosphere: Environmental Changes and Human Risks, edited by: Huggel, C., Carey, M., Clague, J. J., and Kääb, A., Cambridge University Press, Cambridge, UK, 2015.

Driedger, C. and Fountain, A.: Glacier outburst floods at Mount Rainier, Washington state, USA, Ann. Glaciol., 13, 51–55, 1989.

Fountain, A.: Englacial processes, in: Encyclopedia of Snow, Ice and Glaciers, Springer, Dordrecht, the Netherlands, 1253 pp., 2011.

Fountain, A., Jacobel, R., Schlichting, R., and Jansson, P.: Fractures as the main pathways of water flow in temperate glaciers, Nature, 433, 618–621, 2005.

Gardelle, J., Berthier, E., Arnaud, Y., and Kääb, A.: Region-wide glacier mass balances over the Pamir-Karakoram-Himalaya during 1999–2011, The Cryosphere, 7, 1263–1286, doi:10.5194/tc-7-1263-2013, 2013.

Geomer: FloodArea User Manual V. 10.0, 49 pp., Heidelberg, Germany, 2012.

Gulley, J.: Structural control of englacial conduits in the temperate Matanuska Glacier, Alaska, USA, J. Glaciol., 55, 681–690, 2009.

Haeberli, W.: Frequency and characteristics of glacier floods in the Swiss Alps, Ann. Glaciol., 4, 85–90, 1983.

Höhle, J. and Höhle, M.: Accuracy assessment of digital elevation models by means of robust statistical methods, ISPRS J. Photogramm., 64, 398–406, doi:10.1016/j.isprsjprs.2009.02.003, 2009.

Holzer, N., Neckel, N., Buchroithner, M., Gourmelen, N., Colin, J., and Bolch, T.: Glacier variations at Gurla Mandhata (Naimona'nyi), Tibet: a multi-sensoral approach including TanDEM-X, Pléiades and KH-7 Gambit-1, Remote Sens. Environ., submitted, 2015.

Hovden, A.: Who were the sponsors? Reflections on recruitment and ritual economy in three Himalayan village monasteries, in: Tibetans who Escaped the Historian's Net: Studies in the Social History of Tibetan Societies, Vajra Publications, edited by: Ramble, C., Schwieger, P., and Travers, A., Kathmandu, 209–230, 2013.

Huggel, C., Kääb, A., Haeberli, W., Teysseire, P., and Paul, F.: Remote sensing based assessment of hazards from glacier lake outbursts: a case study in the Swiss Alps, Can. Geotech. J., 39, 316–330, 2002.

Huss, M.: Density assumptions for converting geodetic glacier volume change to mass change, The Cryosphere, 7, 877–887, doi:10.5194/tc-7-877-2013, 2013.

ICIMOD: Glacial Lakes and Glacial Lake Outburst Floods in Nepal, Tech. rep., ICIMOD, Kathmandu, 2011.

ICPR: Atlas of flood danger and potential damage due to extreme floods of the Rhine, International Commission on the Protection of the Rhine, available at: http://www.iksr.org/index.php?id=212&L=3 (last access: 17 September 2015), 2001.

James, M. R. and Robson, S.: Straightforward reconstruction of 3D surfaces and topography with a camera: accuracy and geoscience application, J. Geophys. Res., 117, 2156–2202, 2012.

Kääb, A., Berthier, E., Nuth, C., Gardelle, J., and Arnaud, Y.: Contrasting patterns of early twenty-first-century

glacier mass change in the Himalayas, Nature, 488, 495–498, doi:10.1038/nature11324, 2012.

Kääb, A., Treichler, D., Nuth, C., and Berthier, E.: Brief Communication: Contending estimates of 2003–2008 glacier mass balance over the Pamir-Karakoram-Himalaya, The Cryosphere, 9, 557–564, doi:10.5194/tc-9-557-2015, 2015.

Manning, R.: On the flow of water in open channels and pipes. Transactions of the Institution of Civil Engineers of Ireland, Transactions of the Institution of Civil Engineers of Ireland, 20, 161–207, 1891.

Maussion, F., Scherer, D., Mölg, T., Collier, M., Curio, J., and Finkelnburg, R.: Precipitation Seasonality and Variability over the Tibetan Plateau as Resolved by the High Asia Reanalysis, J. Climate, 27, 1910–1927, 2014.

Miehe, G., Winiger, M., Böhner, J., and YILI, Z.: The Climatic Diagram Map of High Asia, Purpose and Concepts, Erdkunde, 55, 94–97, 2001.

NASA: Landsat 7 science data users handbook, NASA, available at: http://landsathandbook.gsfc.nasa.gov/pdfs/Landsat7_Handbook.pdf (last access: 8 September 2014), 2004.

Neckel, N., Kropáček, J., Bolch, T., and Hochschild, V.: Glacier mass changes on the Tibetan Plateau 2003–2009 derived from ICESat laser altimetry measurements, Environ. Res. Lett., 9, 014009, doi:10.1088/1748-9326/9/1/014009, 2014.

Ng, F. and Bjornsson, H.: On the Clague-Mathews relation for jokulhlaups, J. Glaciology, 49, 161–172, 2003.

Ng, F. and Liu, S.: Temporal dynamics of a jökulhlaup system, J. Glaciology, 55, 651–665, doi:10.3189/002214309789470897, 2009.

Nie, Y., Liu, Q., and Liu, S.: Glacial lake expansion in the Central Himalayas by Landsat images, 1990–2010, PLoS ONE, 8, e83973, doi:10.1371/journal.pone.0083973, 2013.

Nuth, C. and Kääb, A.: Co-registration and bias corrections of satellite elevation data sets for quantifying glacier thickness change, The Cryosphere, 5, 271–290, doi:10.5194/tc-5-271-2011, 2011.

O'Connor, J. E., Hardison, J., and Costa, J.: Debris flows from failures Neoglacial-age moraine dams in the Three Sisters and Mount Jefferson wilderness areas, Oregon, Tech. rep., available at: http://pubs.er.usgs.gov/publication/pp1606, 2001.

Paul, F. and Kääb, A.: Perspectives on the production of a glacier inventory from multispectral satellite data in Arctic Canada: Cumberland Peninsula, Baffin Island, Ann. Glaciol., 42, 59–66, 2005.

Peel, M. C., Finlayson, B. L., and McMahon, T. A.: Updated world map of the Köppen-Geiger climate classification, Hydrol. Earth Syst. Sci., 11, 1633–1644, doi:10.5194/hess-11-1633-2007, 2007.

Pfeffer, W. T., Arendt, A. A., Bliss, A., Bolch, T., Cogley, J. G., Gardner, A. S., Hagen, J. O., Hock, R., Kaser, G., Kienholz, C., Miles, E. S., Moholdt, G., Mölg, N., Paul, F., Radić, V., Rastner, P., Raup, B. H., Rich, J., and Sharp, M. J.: The Randolph Glacier Inventory: a globally complete inventory of glaciers, J. Glaciol., 60, 537–551, doi:10.3189/2014JoG13J176, 2014.

Reynolds, J. M., Dolecki, A., and Portocarrero, C.: The construction of a drainage tunnel as part of glacial lake hazard mitigation at Hualcán, Cordillera Blanca, Peru, Geological Society, London, Engineering Geology Special Publications, 15, 41–48, doi:10.1144/GSL.ENG.1998.015.01.05, 1998.

Shi, Y.: Concise Glacier Inventory of China, Shanghai Popular Science Press, Shanghai, 2008.

Shreve, R.: Movement of water in glaciers, J. Glaciol., 11, 205–214, 1972.

Snavely, N., Seitz, S. M., and Szeliski, R.: Modeling the world from internet photo collections, Int. J. Comput. Vision, 80, 189–210, doi:10.1007/s11263-007-0107-3, 2008.

Sundborg, A.: The river Klarälven, a study of fluvial processes, Geografiska Annaler, 38, 125–237, 1956.

Tarboton, D.: A new method for the determination of flow directions and upslope areas in grid digital elevation models, Water Resour. Res., 33, 309–319, 1997.

Vincent, C., Auclair, S., and Meur, E.: Outburst flood hazard for glacier-dammed Lac de Rochemelon, France, J. Glaciol., 56, 91–100, doi:10.3189/002214310791190857, 2010.

Walder, J. S. and Costa, J.: Outburst floods from glacier-dammed lakes: the effect of mode of lake drainage on flood magnitude, Earth Surf. Proc. Land., 21, 701–723, 1996.

Westoby, M., Brasington, J., Glasser, N., Hambrey, M., and Reynolds, J.: "Structure-from-Motion" photogrammetry: a low-cost, effective tool for geoscience applications, Geomorphology, 179, 300–314, doi:10.1016/j.geomorph.2012.08.021, 2012.

Westoby, M. J., Brasington, J., Glasser, N. F., Hambrey, M. J., Reynolds, J. M., Hassan, M. A. A. M., and Lowe, A.: Numerical modelling of glacial lake outburst floods using physically based dam-breach models, Earth Surf. Dynam., 3, 171–199, doi:10.5194/esurf-3-171-2015, 2015.

Wu, C.: VisualSFM: A Visual Structure from Motion System, available at: http://ccwu.me/vsfm/ (last access: 11 November 2014), 2011.

Yao, T.-D., Pu, J., Tian, L., Yang, W., Duan, K., Ye, Q., and Lonnie, G. T.: Recent Rapid Retreat of the Naimona'nyi Glacier in Southwestern Tibetan Plateau, J. Glaciol. Geocryol., 29, 503–508, 2007.